Hydrogen-treated hierarchical titanium oxide nanostructures for photoelectrochemical water splitting

Luca Mascaretti[a,*], Simona Ferrulli[a], Piero Mazzolini[a,b], Carlo S. Casari[a,b], Valeria Russo[a], Roberto Matarrese[c], Isabella Nova[c], Giancarlo Terraneo[b,d], Ning Liu[e], Patrik Schmuki[e,f], Andrea Li Bassi[a,b,*]

[a] Micro- and Nanostructured Materials Laboratory, Department of Energy, Politecnico di Milano, via Ponzio 34/3, 20133, Milano, Italy.

[b] Center for Nanoscience and Technology – IIT@Polimi, via Giovanni Pascoli 70/3, 20133, Milano, Italy.

[c] Laboratory of Catalysis and Catalytic Processes, Department of Energy, Politecnico di Milano, via La Masa 34, 20156, Milano, Italy.

[d] Laboratory of Nanostructured Fluorinated Materials (NFMLab), Department of Chemistry, Materials, and Chemical Engineering "Giulio Natta", Politecnico di Milano, via L. Mancinelli 7, 20131 Milano, Italy.

[e] Department of Materials Science WW4-LKO, University of Erlangen-Nuremberg, Martenstrasse 7, 91058, Erlangen, Germany.

[f] Department of Chemistry, King Abdulaziz University, Jeddah, Saudi Arabia.

***corresponding author**

Andrea Li Bassi

Micro- and Nanostructured Materials Laboratory, Department of Energy, Politecnico di Milano
Via Ponzio 34/3, 20133, Milano, Italy
andrea.libassi@polimi.it

Luca Mascaretti

Micro- and Nanostructured Materials Laboratory, Department of Energy, Politecnico di Milano
Via Ponzio 34/3, 20133, Milano, Italy
luca.mascaretti@polimi.it

Abstract

Hierarchical titanium oxide nanostructures were synthesized by Pulsed Laser Deposition (PLD) and investigated as photoanodes for photoelectrochemical water splitting. An explorative combined approach to enhance TiO_2 performance was based, on the one hand, on the employment of hydrogenation treatments with the aim of improving quantum efficiency and extending light absorption to the visible range; on the other hand, on the optimization of morphology and structure, to increase light harvesting and charge separation/transport. This approach was pursued by depositing at a fixed background pressure with variable oxygen content (to control the growth morphology and structure) and by annealing in a Ar/H_2 mixture (in substitution of or in combination with air annealing), in order to induce crystallization to the anatase structure and reduction/hydrogenation of the material. Morphology, structure and optical properties were investigated by SEM, Raman spectroscopy, X-ray diffraction and UV-visible-IR spectroscopy. An optical absorption tail towards the visible range appeared after Ar/H_2 annealing, without any significant modification of the nanoscale structure after the different thermal treatments. Photocurrent measurements under solar simulator illumination showed a noteworthy increase of photoresponse for Ar/O_2-deposited samples with air annealing followed by Ar/H_2 annealing. These findings can be ascribed to the combination between an improved charge transport of TiO_2 deposited in low-O_2 atmosphere and a hydrogenation effect on the nanostructures surface layers, leading to improved quantum efficiency.

Keywords

TiO_2; hierarchical nanostructures; pulsed laser deposition; hydrogen treatment; photoelectrochemical water splitting.

1. Introduction

Hydrogen has been suggested as a possible alternative energy carrier to fossil fuels, since its combustion reaction leads only to water vapor; additionally, it is possible to produce it without greenhouse gases as byproducts exploiting the energy of solar radiation [1]. One promising way in this direction, although far from commercial application, is by means of the so-called photoelectrochemical (PEC) water splitting, in which, most commonly, a photoanode semiconductor material, immersed in water and electrically connected to a cathode, is illuminated by solar light and promotes the decomposition of water into molecular oxygen and hydrogen [2].

This phenomenon was firstly reported in 1972 by Fujishima and Honda using a titanium dioxide (TiO_2) photoanode [3]. Today, nanostructured TiO_2 is still the most investigated material thanks to its activity, low-cost, non-toxicity and high chemical stability [4]. Nevertheless, it suffers from two main limitations: poor light absorption in the visible region and limited quantum efficiency for the water splitting process [4]. To overcome these issues, two main strategies have been proposed so far in literature: i) tuning the material structure and morphology at the nanoscale, in order to enhance the active surface, improve light harvesting and minimize charge recombination, and/or ii) doping or sensitization, to shift the absorption towards the visible light [2,4].

Investigations concerning the first approach have been undertaken in several ways. Notably, one-dimensional (1D) or quasi-1D nanostructures have been recently considered to the anisotropic morphology, desirable for a preferential electron transport towards the electrical contact, and, at the same time, the large surface area with tunable porosity at the nanoscale, favoring the infiltration of molecules as well as effective light scattering [5–7]. For instance, extensive research has been devoted to TiO_2 nanotube arrays, thanks to their high surface-to-volume ratio, ordered geometry and simple production process by electrochemical anodization [5], and to quasi-1D hierarchical nanostructures, due to their increased light trapping capability [8]. The latter can be prepared, for instance, by controlling the process parameters of pulsed laser deposition (PLD), an effective and versatile physical vapor deposition technique able to produce thin films of several materials with controlled morphological, structural and functional properties [9,10]. Indeed, TiO_2 hierarchical nanostructures prepared by PLD have been studied by some of us as photoanodes for the oxidation of organic molecules [11], for dye-sensitized solar cells [12,13] and, recently, for photoelectrochemical water splitting [14].

Research aimed at shifting absorption to the visible range has also been extensively developed. Typically, the solar absorption of TiO_2 increases by adding a controlled amount of metal or non-metal impurities capable to generate donor or acceptor states in the bandgap [2]. Recently, a different strategy has been proposed by Chen and Mao [15] by producing a modified form of TiO_2 with a narrowed bandgap. This material, called *"black titania"*, was obtained by treating anatase nanocrystals in a pure hydrogen atmosphere at high temperature and pressure. As black titania showed a significantly increased photocatalytic activity for water splitting with respect to pure TiO_2, several works have been devoted to the synthesis and control of this material. In most of them, TiO_2 nanopowders have been considered and various experimental methods have been employed in order to obtain black titania; accordingly, the results depend on the experimental procedure [16]. Moreover, despite some theoretical investigations [17], an accurate and complete comprehension of the atomic-scale structural changes and of the physical mechanisms involved in

hydrogenation and leading to the striking functional properties of black titania has not been achieved yet.

Recent investigations have shown encouraging results in the attempt to combine an suitable morphology with extension of the photoresponse to the visible range, some example being hydrogen treatment on rutile nanowires [18], vacuum annealing of wire-in-tube nanostructures [19] and hydrogen treatment on nanotube arrays [20]. However, many open questions still need to be addressed to reach a full control of morphology and composition to develop this combined approach as a reliable strategy for the realization of effective TiO_2 photoanodes.

Here we develop photoanodes based on titanium oxide hierarchical nanostructures and we study in detail the effect of the deposition atmosphere and of thermal treatments in a Ar/H_2 mixture at atmospheric pressure on the photoelectrochemical water splitting performances, with the aim of investigating and understanding the relation between structural properties and photoresponse.

2. Experimental

2.1 Synthesis of TiO_2 photoanodes

TiO_2 nanostructured films have been deposited by ablating a TiO_2 target with a ns-pulsed laser (Nd:YAG, 2nd harmonic, λ = 532 nm, repetition rate 10 Hz, pulse duration 5-7 ns). The laser fluence on the target was set at about 3.5 J/cm^2 and the laser pulse energy was 170 mJ. Silicon (100), soda-lime glass and titanium plates were used as substrates, mounted on an off-axis rotating sample holder at a fixed target-to-substrate distance of 50 mm. All the substrates were kept at room temperature and titanium plate substrates of 2×1 cm^2 were half masked during deposition to leave a clean surface for electrical contacts for photoelectrochemical measurements. The deposited mass was fixed at about 0.3 mg/cm^2, as estimated from quartz microbalance measurements; the deposition rate ranged between 6 and 16 nm/min. The depositions were performed at a fixed background gas pressure of 5 Pa in three different gas atmospheres: pure oxygen, Ar/O_2 mixture (50%-50%) and Ar/H_2 mixture (97%-3%). We selected a deposition pressure of 5 Pa, with a nominal thickness of about 1.4 μm, according to the best results obtained in a previous work [14], in which some of us investigated the morphology dependence of the photoelectrochemical response of TiO_2 nanostructured films deposited by PLD.

Post deposition annealing treatments were performed in a Lenton muffle furnace in air at 500°C (4°C/min heating ramp, 2 hours dwell). This "standard" air annealing was either followed by or substituted with a thermal treatment in a Ar/H_2 (97%-3%) mixture at atmospheric pressure performed in a home-made furnace at 500°C (10°C/min heating ramp, 3 hours dwell).

2.2 Morphological and structural characterization

SEM analyses (top view and cross-sectional) were performed on samples grown on silicon substrates with a ZEISS Supra 40 FEG-SEM without any sample preparation.

Raman spectra were collected from samples grown on silicon or glass substrates using a Renishaw InVia micro Raman spectrophotometer with 514.5 nm laser excitation wavelength and power on sample of about 1 mW.

X-Ray diffraction patterns were collected using a Bruker D8 Adavance X Ray diffractometer, operating in reflection mode with Ge-monochromated Cu Kα1 radiation (λ = 1.5406 Å) and a linear position-sensitive detector; with a 2θ range 10−70°, a step size 0.038° and time/step 1.5 sec. Samples were mounted in sample holder with motorized z-position (4.3 mm). Diffraction patterns were collected at room temperature. The peak position and the full-width at half maximum (FWHM) of the peaks were then obtained using TOPAS software (Bruker). The crystallite sizes were estimated through the Scherrer formula [21].

Optical transmittance (in the range 250 – 2000 nm) and reflectance spectra (in the range 290 – 600 nm) were evaluated with a UV-vis-NIR PerkinElmer Lambda 1050 spectrophotometer with a 150 mm diameter integrating sphere. All the acquired spectra were normalized with respect to the glass substrate contribution by setting to 1 the intensity at the glass/film interface.

2.3 Photoelectrochemical experiments

Photoelectrochemical (PEC) measurements were carried out in aqueous KOH solution (0.1 M) with a three-electrode cell equipped with a flat quartz window. TiO_2 films on Ti substrate photoanodes (working area of 1 cm^2) were used as the working electrode while a platinum grid and a saturated calomel electrode (SCE) were used as counter and reference electrode, respectively. The light source was a solar simulator (Lot Quantum Design LS0306) equipped with a 300 W xenon arc lamp and AM1.5G filter (Lot Quantum Design LSZ389). A light intensity of 100 mW/cm^2 was measured prior to the experiments using a light meter HD2302.0 (Delta OHM). The performance of the TiO_2 photoanodes was evaluated by measuring the photocurrents under an external bias [22–25], provided by a potentiostat (Amel 7050) performing potential ramps from −0.8 V to about 0.5 V, with a scan rate of 5 mV/s. PEC measurements were also performed under constant light illumination and fixed bias potential (0.4 V) for 6 hours, in order to evaluate the photoanodes stability [26–28].

Photocurrent spectral quantum efficiency was measured in the range 300- 600 nm at an applied potential of 0.5 V using a three electrode arrangement (Ag/AgCl, 3 M KCl, as reference and Pt as counter electrode) in an electrochemical cell equipped with a quartz glass window in 0.1 M Na_2SO_4 solution. The illumination setup consisted of an Oriel 6356 150 W Xe arc lamp as a light source and an Oriel XCornerstone 7400 1/8 monochromator.

3. Results and discussion

The adopted strategy to obtain hydrogenated/reduced hierarchical TiO_2 nanostructures and to study the corresponding effect on the photoelectrochemical activity is based on the control of both deposition and annealing conditions. On the one hand, three deposition atmospheres have been selected, keeping the total pressure at 5 Pa, as follows:

- pure oxygen ("**O_2-TiO_2**", reference);
- Ar/O_2 (50%-50%) mixture ("**Ar/O_2-TiO_2**");
- Ar/H_2 (97%-3%) mixture ("**Ar/H_2-TiO_2**").

The last two approaches were intended as a means to induce oxygen sub-stoichiometry and/or hydrogenation in a partially reducing environment, directly in the synthesis step. On the other hand, three post-deposition thermal treatments have been tested for each of the deposition conditions, as follows:

- air, 500°C, 2 hours ("**Air**", reference);
- Ar/H_2 (97%-3%) atmosphere, 500°C, 3 hours ("**Ar/H_2**") at environmental pressure;
- "double treatment": Air annealing followed by Ar/H_2 ("**Air+Ar/H_2**").

For each deposition condition (i.e. background atmosphere) we evaluated the effect of the three different annealing procedures on twin samples deposited in the same PLD experimental run. Accordingly, all the samples have been characterized from a morphological, structural and optical point of view and, finally, tested in a photoelectrochemical cell.

3.1 Photoanode structure and morphology

The morphology of as-deposited titanium oxide films obtained in different background atmospheres, keeping the total pressure fixed at 5 Pa, is presented in the SEM images in Fig. 1. The O_2-TiO_2 film surface (Fig. 1A) exhibits a granular appearance and a nanoscale porosity; cross-sectional images (Figs. 1B, C) show a morphology organized in vertically-oriented nanostructures, which, at higher magnification (Fig. 1C), appear to be composed by nanoparticles. Similarly, the Ar/O_2-TiO_2 film (Fig. 1D) shows a morphology characterized by oriented porous columnar structures composed of nanoparticles. Conversely, the Ar/H_2-TiO_2 film (Fig. 1E) grows denser and more compact and their thickness is lower (i.e. 1 μm instead of 1.4 μm).

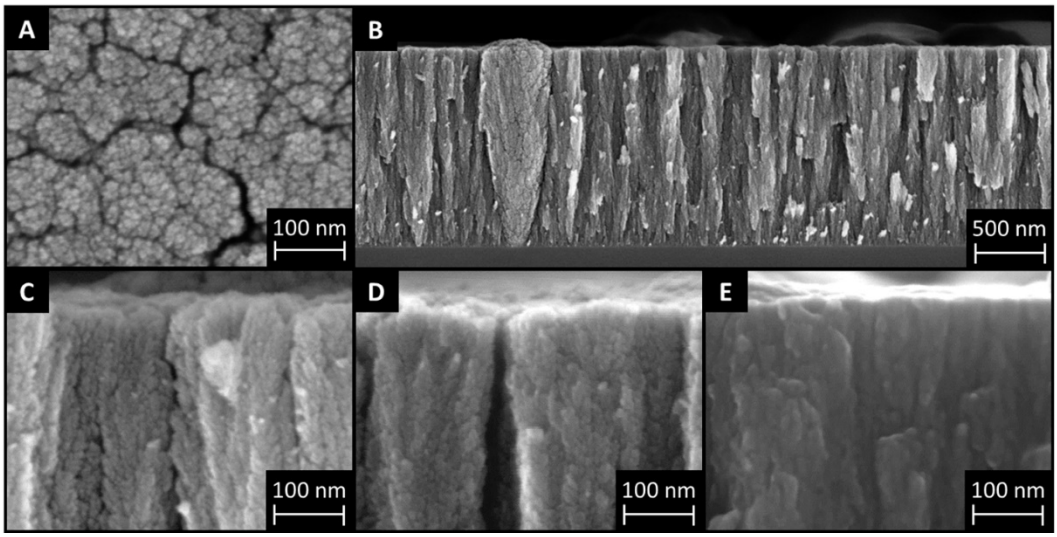

***Figure 1**: Top-view and cross-sectional SEM images of TiO_2 samples as-deposited with PLD. **A)** O_2-TiO_2 (top view); **B)** O_2-TiO_2 (cross section; the full film is visible, having a thickness of 1.4 µm); **C)** O_2-TiO_2 (higher magnification); **D)** Ar/O_2-TiO_2; **E)** Ar/H_2-TiO_2.*

Raman spectra allow to investigate the degree of structural order and the oxide phase. As shown in Fig. 2, all the Raman spectra of as-deposited films are characterized by broad bands, typical of highly disordered materials, so that the overall shape of spectra and band broadness do not allow to determine the oxide phase. O_2-TiO_2 and Ar/O_2-TiO_2 films show similar spectra with three very large features, while Ar/H_2-TiO_2 shows a spectrum with even broader features, which is an indication of a higher degree of local disorder. This difference is probably related to the lower oxygen content in the Ar/H_2-TiO_2 sample induced by the deposition in a reducing atmosphere [29].

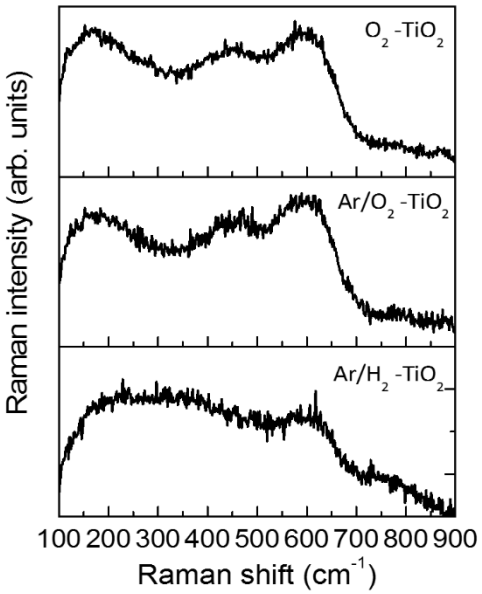

***Figure 2:** Raman spectra of as-deposited TiO_2 samples with different background gas: pure O_2 (top), Ar/O_2 mixture (middle) and Ar/H_2 mixture (bottom).*

The observed morphological effects are related to clustering and diffusion phenomena occurring in the expanding ablation plume during the deposition process. It can be expected that O_2 and Ar/O_2

atmospheres affect the growth in a very similar way, considering that the molecular mass of O_2 and Ar are very similar (and thus the associated elastic scattering processes [30]). On the other hand, deposition in Ar/H_2 results in a different morphology, possibly related to different chemical reactions occurring during expansion, thus affecting the dynamics of the plume; this likely leads to a different kinetic energy of the deposited species and, possibly, to a strongly under-oxidized material.

All the films have been exposed to post-deposition thermal treatments and morphological and structural effects have been investigated. We here discuss these effects for Ar/O_2-TiO_2 samples, which showed the best photoelectrochemical response (as discussed below); a very similar behavior has been observed for O_2-TiO_2 and Ar/H_2-TiO_2 films (see Supporting information).

The morphology of Ar/O_2-TiO_2 film before and after annealing treatments is shown in SEM images of Fig. 3. The overall morphology after any thermal treatment does not change; however, the nanostructure organization becomes more evident, together with a partial merging between nanoparticles constituting the film, due to a sintering effect induced by annealing. This leads to an increase in coalescence and connectivity among the nanoparticles. The sintering effect is particularly evident upon annealing in air; this could also be related to the slower heating/cooling rate of the muffle furnace.

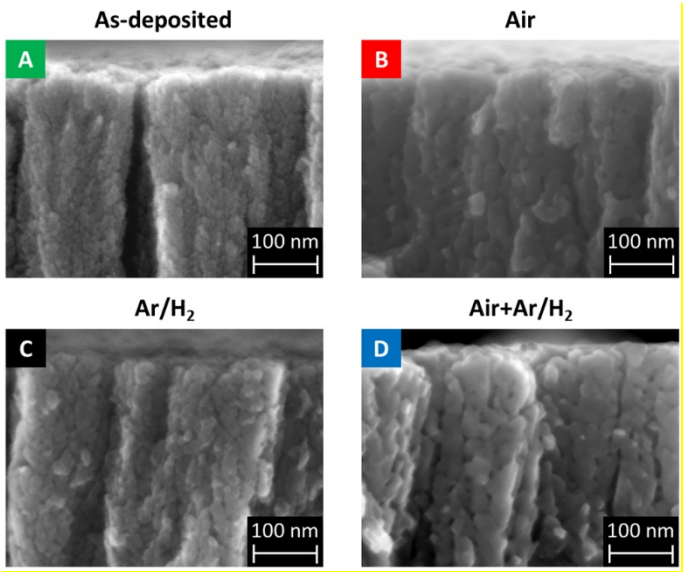

Figure 3: *SEM images of Ar/O_2-TiO_2 films.* ***A)*** *As-deposited;* ***B)*** *Air annealed;* ***C)*** *Ar/H_2 annealed;* ***D)*** *Air+Ar/H_2 annealed.*

The crystalline structure of the annealed samples was first investigated by means of Raman spectroscopy (as shown in Fig. 4). From the comparison with the as-deposited films (Fig. 2), it is evident that all the annealing treatments induce crystallization in the anatase phase. Indeed, the five characteristic peaks of this phase at 144, 198, 399, 517 and 638 cm^{-1} are present in all the spectra, while the sixth weak A_{1g} active mode expected at 513 cm^{-1} is covered and merges into the peak at 517 cm^{-1} [31]. Moreover, no significant variation of position or width of the peaks is observed; therefore, we can exclude relevant effects related to quantum confinement [32,33], large defectivity [34] or poor O stoichiometry [32,35]. The same behavior, i.e. crystallization to anatase phase

independent from the adopted thermal treatment, has been observed also for samples deposited in a different background atmosphere (pure O_2 and Ar/H_2, see Supporting information).

In addition, a photoluminescence (PL) background appears under the Raman peaks for Ar/H_2- and $Air+Ar/H_2$-annealed films, but not for the Air-annealed one. This is evident from Fig. 4B, in which PL spectra excited by the same laser line used for Raman measurements (514.5 nm, i.e. 2.41 eV, thus smaller than the bandgap) are reported; a large band is observed in the spectral region from 550 to 900 nm (1.3-2.3 eV), composed by a few components. Since these PL features are absent for the Air-annealed film, we assume that they are related to defect levels in the oxide gap induced by the hydrogenation treatment, such as O vacancies or Ti^{3+} sites, as reported for instance for hydrogen-treated TiO_2 nanoparticles [36]; indeed, these defects are typically foreseen in reduced TiO_2 materials [37]. However, the exact nature of H-induced defects and disorder in black titania is still a partially open issue [16,38], and further investigation is necessary to assess the precise origin of the observed PL and the related involved defects and energy levels (for instance with low temperature PL measurements). In our case, a photoluminescence background in Raman spectra can be considered and used as an indication of radiative recombination through defect states, induced by thermal treatments in a reducing atmosphere; as such, these defects could be present only in a limited amount in air-annealed films, thus not giving rise to a PL signal.

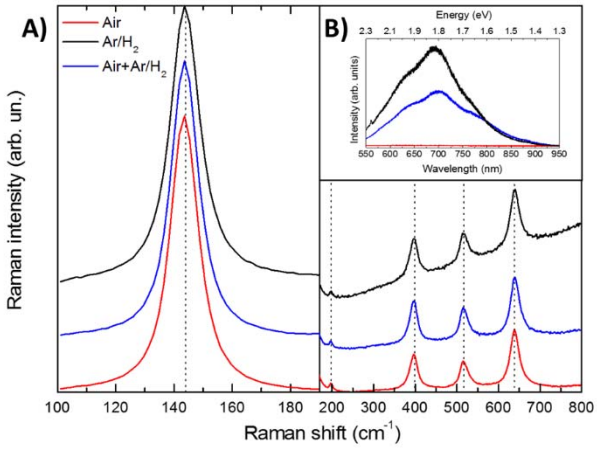

Figure 4: ***A)*** *Raman spectra of annealed Ar/O_2-TiO_2 samples (red: Air; blue: $Air+Ar/H_2$; black: Ar/H_2). Spectra are separated in two panels with arbitrary intensity units because the peak at 144 cm^{-1} is largely more intense than all the other peaks.* ***B)*** *Photoluminescence spectra (acquired at room temperature with excitation wavelength of 514.5 nm) of annealed Ar/O_2-TiO_2 samples (same colors as* ***A****).*

Further information on the crystalline structure has been obtained by means of X-ray diffraction (Fig. 5) showing that the as-deposited films are amorphous, while once annealed they become crystalline with anatase phase, in agreement with the observations from Raman spectroscopy. The crystal domain size, estimated through the Scherrer formula for the (004) peaks, is between 30 and 40 nm, similarly to the estimate made by SEM observations.

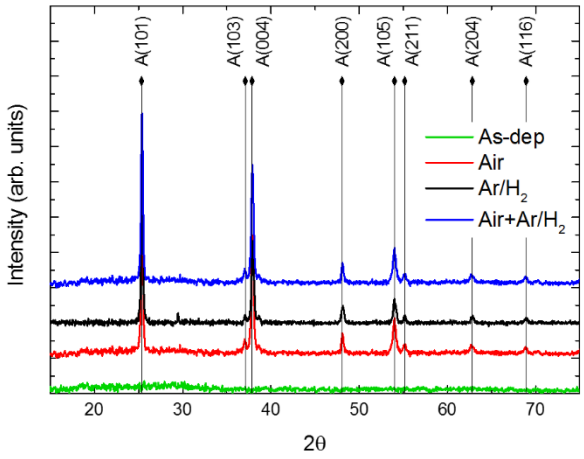

Figure 5: *XRD spectra of as-deposited and annealed Ar/O_2-TiO_2 films on glass substrates (green: as-deposited; red: Air; black: Ar/H_2; blue: Air+Ar/H_2).*

To investigate the optical absorption properties of the annealed Ar/O_2-TiO_2 films, transmittance and reflectance spectra in the UV-vis-NIR range are shown in Fig. 6. First, we observe that the three annealing treatments result in a different color of the films, as visible to the unaided eye: the Air-annealed one is white, the Ar/H_2-annealed is dark-yellow and the Air+Ar/H_2-annealed one is grey (see inset of Fig. 6). This qualitative color difference is experimentally confirmed by a change in the transmittance curves, especially in the visible region: in proximity of the optical bandgap, the absorption edge is smoother for the samples annealed in Ar/H_2 with respect to the sample only annealed in air. For all the samples the haze factor, evaluated as the ratio between the diffuse and the total components of the transmittance, is between 20% and 40% (see Supporting information). Absorbance spectra are obtained from transmittance and reflectance measurements in the bandgap region (Fig. 6B). In this case, the Ar/H_2-annealed film shows a more pronounced absorption tail in the visible range; however, the bandgap of all the samples, evaluated with the Tauc plot method, is almost unchanged, about 3.2 eV, which is the typically expected value of anatase (see Supporting information).

The appearance of the absorption tail in the visible range without a change in the bandgap value is related to the presence of a limited amount of defect states in the bandgap, introduced by annealing in Ar/H_2 atmosphere, or to surface states. The presence of these defects is supported by photoluminescence spectra, which suggest radiative emission upon excitation with photon energy below the bandgap (2.4 eV). However, a precise identification of these defect states would require specific investigations and is beyond the scope of the present work.

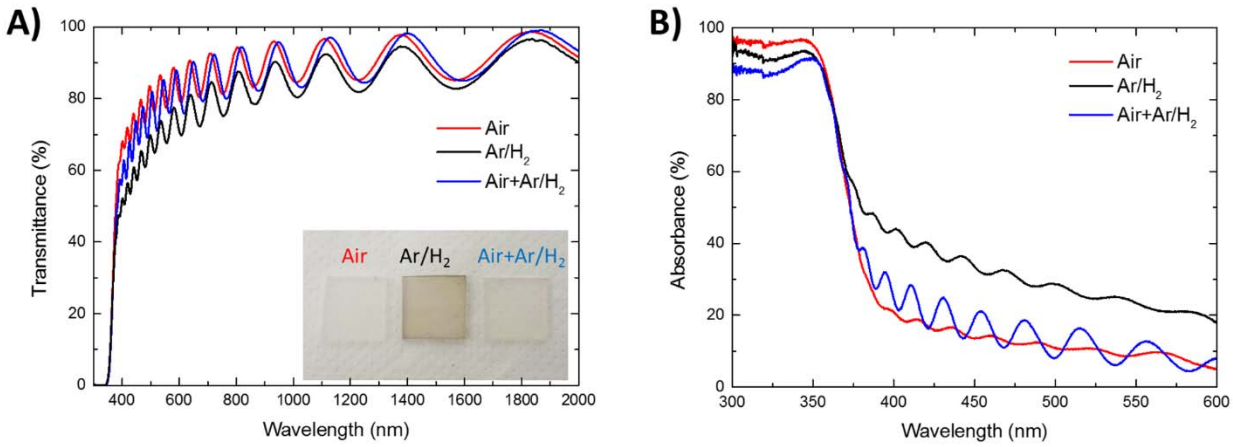

Figure 6: *Optical analysis of annealed Ar/O_2-TiO_2 films (red: Air; black: Ar/H_2; blue: $Air+Ar/H_2$).* ***A)*** *Transmittance curves;* ***B)*** *absorbance curves.*

3.2 Photoelectrochemical properties

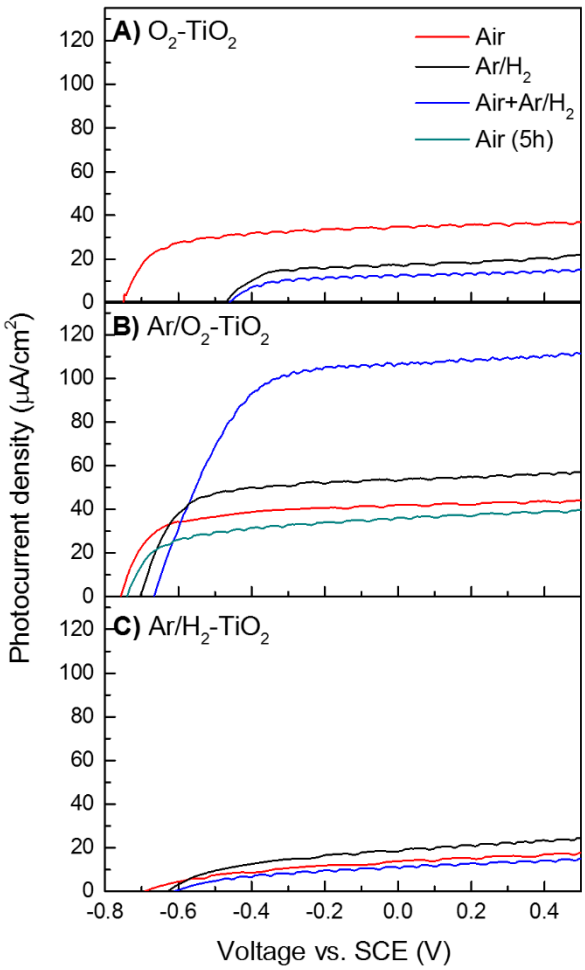

Figure 7: *Effect of the annealing treatment on the photoelectrochemical behavior for TiO_2 photoanodes produced at 5 Pa of pure O_2 (**A**), Ar/O_2 atmosphere (**B**) and Ar/H_2 atmosphere (**C**); J−V curves obtained with a scan rate of 5 mVs^{-1}. Each color corresponds to an annealing treatment, as follows: red, Air; black, Ar/H_2; blue, $Air+Ar/H_2$; green, Air for 5 hours.*

The effect of the annealing treatments on the photoresponse of films deposited in pure O_2, Ar/O_2 and Ar/H_2 mixture, evaluated with photocurrent measurements, is presented in Figs. 7A, B and C, respectively. All the samples exhibit negligible anodic current (less than 5 μA cm^{-2}) under dark conditions (not shown) over all the investigated potential range, which indicates that insignificant photoelectrochemical water oxidation occurred at the anodes surface. On the contrary, upon illumination, photocurrent generation is observed.

For the O_2-TiO_2 photoanodes (Fig. 7A), the best performances are associated with the film annealed in air: photocurrent onset is observed at approximately −0.75 V; then the photocurrent density gradually increases with the applied potential, because of the efficient charge carriers separation under the effect of the applied bias [39–41], until a saturated photocurrent density of ca. 40 μA cm^{-2} is observed. The photoresponse decreases for these samples after Ar/H_2 or $Air+Ar/H_2$ annealing: in these cases, the photocurrent onset is observed at a higher potential value (about −0.45 V), and a lower saturated photocurrent density is measured (i.e. reaching values near 20 and 15 μA cm^{-2} at 0.5 V, respectively), which suggests a less efficient generation and transfer of photogenerated charge carriers and major recombination losses, as well [42–44].

In the case of Ar/O_2-TiO_2 photoanodes (Fig. 7B), the film annealed with a double $Air+Ar/H_2$ treatment outperforms those annealed in air and Ar/H_2. Indeed, it shows the highest photocurrent densities through the entire potential window, and the saturated photocurrent reaches a value of 110 μA cm^{-2} at 0.5 V, which represents a 3-fold increase of the photocurrent response if compared to the other thermal treatments. As a control experiment, Fig. 7B shows also the results obtained over a Ar/O_2-TiO_2 sample annealed in air for 5 hours instead of 2 hours, as for all the other air-annealed films. As it clearly appears, a photocurrent density comparable to that of the 2-hours air-annealed sample is attained, thus indicating that the increase of photocurrent observed in the case of the double-treated photoanode is not related to the total annealing time, but it likely depends on the hydrogenation treatment.

Finally, the effect of the annealing treatments was also evaluated for Ar/H_2-TiO_2 films (Fig. 7C); in this case we observe that the photocurrent is low and the results show a negligible effect of the different annealing conditions on the photoactivity.

In order to gain information on the effect of the background deposition gas on the photoresponse, Fig. 8 shows the variation of the photocurrent density values recorded at 0.4 V for the films deposited in pure oxygen, Ar/O_2 and Ar/H_2 atmospheres as a function of the different annealing treatments. Clearly, regardless of the annealing conditions, the photoanodes deposited in Ar/O_2 atmosphere always lead to a higher photoresponse than those deposited in pure oxygen and Ar/H_2 atmosphere. Moreover, among the Ar/O_2-TiO_2 films, the most promising thermal annealing is the $Air+Ar/H_2$ treatment. Conversely, the least effective photoanodes are those prepared under Ar/H_2 atmosphere.

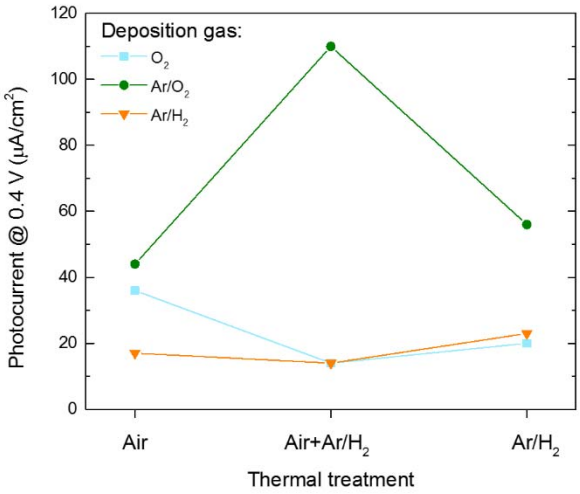

Figure 8: *Photocurrent density, recorded at 0.4 V vs. SCE for photoanodes deposited in pure oxygen (■), in Ar/O_2 atmosphere (●) and Ar/H_2 atmosphere (▼), as a function of the different annealing treatments.*

The films' behavior has been further examined by considering the photoconversion efficiency (η%), which has been calculated according to equation (1) [45,46]:

$$\eta\ (\%) = (J\ (E^{\circ} - |\ E_{app}\ |))/I*100 \qquad (1)$$

where J is the photocurrent density (μA cm^{-2}), E°=1.23V is the standard reversible potential for water splitting, $|\ E_{app}\ |$ is the applied potential (evaluated as the difference between the bias potential and the OCV under the irradiated power light), and I is the incident light power density. Accordingly, photoconversion efficiency is particularly useful in the analysis of electrically driven photo-processes, as in the present case, because it takes into account not only the power light but also the external potential applied to the electrode. Photoconversion efficiency as a function of potential is shown in Fig. 9 for the different photoanodes annealed in Air (A), Air+Ar/H_2 (B) and Ar/H_2 (C). As it clearly appears, the highest photoconversion efficiencies are found for films deposited in Ar/O_2 atmosphere (green lines), followed by those deposited in pure O_2 (light blue) while the lowest values are found for samples deposited Ar/H_2 atmosphere (orange lines). The maximum photoconversion efficiency of ca. 0.095% is obtained for the Ar/O_2-TiO_2-Air+Ar/H_2 photoanode (deposited in Ar/O_2 and annealed with double treatment, see Fig. 9B).

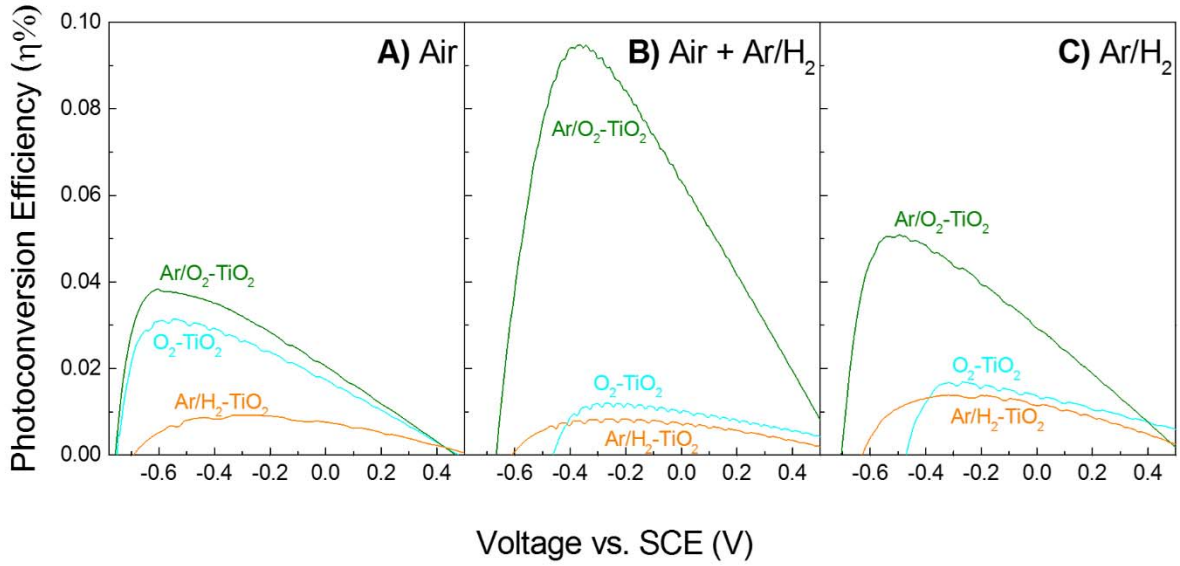

Figure 9: *Photoconversion efficiency for photoanodes annealed in Air (**A**), Air+Ar/H₂ (**B**) and Ar/H₂ (**C**) deposited in pure oxygen* (light blue lines)*, in Ar/O₂ atmosphere* (green lines) *and Ar/H₂ atmosphere* (orange lines).

Finally, the photostability of the Ar/O2-TiO2 films (i.e. the photoanodes with the best performances) was further investigated. Fig. 10 shows the photocurrents measured over time with applied bias potential of 0.4 V for the samples after Air annealing, Ar/H2 annealing and Air+Ar/H2 annealing. In line with the above results, the sample annealed with Air+Ar/H2 treatment shows the highest photocurrent results and, notably, possesses the highest photostability. As a matter of fact, after 6 h of continuous illumination the photocurrent drops within about 5% vs. 15% and 20% for samples annealed in Air and Ar/H2, respectively. Moreover, the photostability of this photoanode was further confirmed by photocurrent measurements over several months, which showed very similar results as those presented in Fig. 7 (not shown).

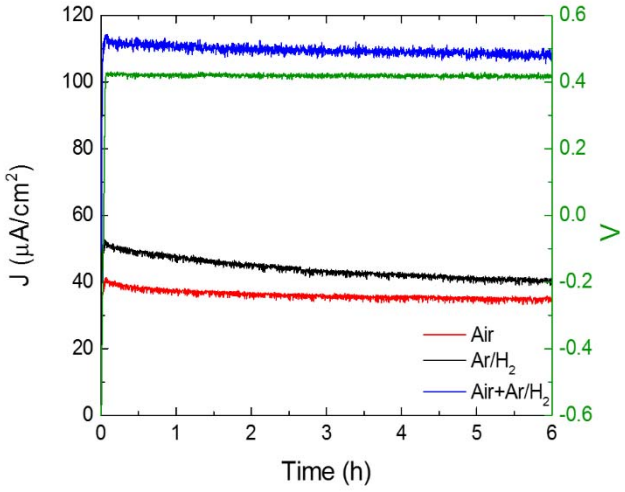

Figure 10: *Photostability of annealed Ar/O₂-TiO₂ photoanodes measured by photocurrent over time with applied bias potential of 0.4 V vs SCE.*

3.3 Discussion

We focused our investigation on the effect of hydrogenation/reduction treatments (during or post-deposition) on the photoelectrochemical properties of hierarchical nanostructured titanium oxide layers. The morphology, which usually depends on the deposition pressure, was kept fixed, as it is optimized in terms of available surface area (of the order of tens of m^2/g) and light scattering performance as a result of previous investigation on similar structures [14].

The findings reported above clearly show that the deposition atmosphere composition and the annealing atmosphere/procedure strongly influence the photocatalytic performances. An explanation of the observed features is not straightforward, also considering that the precise effect of hydrogenation on the atomic scale structure (and thus on the electronic/optical properties) strongly depends on the experimental procedure and is still debated in the current literature [38].

Considering the most active film emerging from photoelectrochemical experiments, i.e. Ar/O_2-TiO_2-$Air+Ar/H_2$ (Fig. 7), useful information comes from the measurement of the photocurrent spectral quantum efficiency (incident photon-to-current efficiency, IPCE, see Fig. 11), which was measured also for Ar/O_2-TiO_2-Air as a reference.

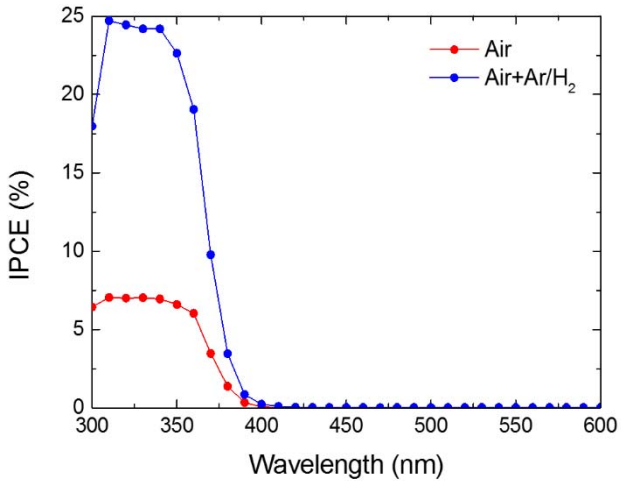

Figure 11: *IPCE spectra of annealed Ar/O_2 samples (black: Air; red: $Air+Ar/H_2$).*

IPCE spectra confirm the beneficial effect of the double annealing (i.e. hydrogenation+air annealing), leading to a significant improvement by a factor > 3. This effect, however, cannot be attributed to the slightly increased absorption in the visible range (i.e. to a small "blackening" effect, see Fig. 6); instead, only quantum efficiency in the UV range is significantly improved.

Structural characterizations (Raman, XRD) and absorption/photoluminescence spectra for all the investigated films point to a material characterized by an assembly of nanoparticles with a crystalline (anatase) core, with hardly detectable disorder or defects confined to the nanoparticles' surface layers. In the recent literature on black titania, indeed, theoretical and experimental evidences show that various defects can be formed depending on the hydrogenation/reduction procedure, such as oxygen vacancies/Ti^{3+} sites, surface disorder, Ti-OH and Ti-H bonds [16,38]. As a consequence, these defects induce electronic states in the bandgap, which can act as trapping sites for photogenerated charges, retarding their recombination [38]. In addition, an improvement in

electrical conductivity has also been suggested as an effect arising from any hydrogenation/reduction treatment of TiO_2 thin films [47].

In our case, the hydrogenation annealing step leads to a significant beneficial effect only if preceded by annealing in air, which is fundamental because it leads not only to crystallization, but also to significant sintering between nanoparticles, as shown in Fig. 3, thus reducing defects/recombinations and improving electron mobility through the formation of crystalline vertical channels (with reduced grain boundaries), where electrons can be efficiently transported to the external circuit, as observed with TEM in previous works [13,48].

The improvement of the photocatalytic performance upon the second annealing step in Ar/H_2 is instead consistent with a hydrogenation effect limited to the particle surface. It is out of the scope of this work to investigate the specific role of hydrogen at the atomic scale, i.e. whether it just provides reducing conditions for the formation of O vacancies/Ti^{3+} sites, or if H terminations play an active role in the photocatalytic process. Indeed, preliminary XPS measurements on the most promising film (Ar/O_2-TiO_2-Air+Ar/H_2) did not point out a clear difference from a reference film (Ar/O_2-TiO_2-Air, not shown). In any case, even though visible absorption is enhanced (Fig. 6), IPCE spectra indicate that hydrogenation is somehow beneficial for improving efficiency in the UV by reducing recombinations or improving charge transport, in agreement with what observed in other works [18,47,49,50].

We now consider the effect of the initial deposition atmosphere on the functional performance of the material. The air annealing step is expected to heal sub-stoichiometry or crystalline defects that may arise from a deposition in oxygen-poor atmosphere; indeed, structural characterization indicates no detectable difference between samples deposited in all the explored atmospheres. However, we make the hypothesis that slight differences, probably related to a small O deficiency in the nanoparticle core and leading to better conduction, are important in terms of photocatalytic performance, so that a *"memory"* effect (with respect to deposition atmosphere) is clear in our results, and particularly for the best performing sample. In fact, a double treatment on TiO_2 deposited in O_2 or in Ar/O_2 leads to completely different results (see Fig. 8).

In particular, the Ar/H_2-deposited samples show the lowest photoresponse (also if we increase the deposition pressure in order to obtain a more open morphology, similar to the O_2- and Ar/O_2-TiO_2 samples; see Supporting information); this can be understood considering that the oxygen deficiency during the deposition process is too high with respect to deposition in Ar/O_2 mixture, as discussed above.

In any case, these observations point to the possibility of finely tuning the deposition atmosphere composition (prior to the annealing procedure), or to exploit the use of metallic Ti targets (instead of TiO_2) for a fine adjustment of the O-deficiency and thus of the material functional properties.

4. Conclusions

Hierarchical TiO_2 nanostructured films have been studied as photoanodes for photoelectrochemical water splitting and the controlled introduction of composition/crystalline defects into the material, in order to increase its photoresponse, was explored both during the deposition step and with annealing in a Ar/H_2 mixture at atmospheric pressure. Thermal treatments in the presence of hydrogen do not affect the overall morphology and structure of the material, but they induce the onset of an absorption tail in the visible range and they influence the material photoactivity; however, the material functional properties are also affected by the deposition gas employed (a sort of "*memory* effect"). It was found that some shortage of oxygen in the deposition step as well as a double thermal treatment (in air and, subsequently, in the Ar/H_2 mixture) lead to a clear enhancement in TiO_2 photoresponse with respect to all the other investigated conditions.

Further optimization of the material is foreseen, both by considering a fine tuning of the deposition atmosphere and by considering other reducing annealing conditions, such as in vacuum, which may help to understand what is the specific role of hydrogen, or in high-pressure pure hydrogen, as typically done for obtaining black titania. However, we would like to underline that the development of low-ambient pressure treatments with a low H_2 content may have an intrinsic interest in view of application development. Indeed, annealing in Ar/H_2 atmosphere have already been proposed for other nanostructures for the application in lithium-ion batteries [51,52] and for photoelectrodes [53].

The obtained results and the manifold improvement possibilities support the promising expectations on the use of hierarchical nanostructures of TiO_2 or other oxides for PEC experiments, as well as other applications, such as photoanodes for solid-state photoelectrochemical solar cells.

Associated content

Supporting information.

O_2-TiO_2 and Ar/H_2-TiO_2 films: SEM images, Raman spectra and optical spectra; Ar/O_2-TiO_2 film: haze factor spectra and Tauc plot curves; Ar/H_2-TiO_2 film deposited at 10 Pa: SEM images, Raman spectra and photocurrent density curves.

Author information

Corresponding author.

* E-mail: andrea.libassi@polimi.it. Tel. +390223996316.

* E-mail: luca.mascaretti@polimi.it. Tel. +390223996347.

Notes. The authors declare no competing financial interest.

Acknowledgements

We thank G. Bussetti for XPS measurements. L. M. wishes to thank S. Perissinotto and L. Passoni for their aid in optical measurements.

Graphical abstract

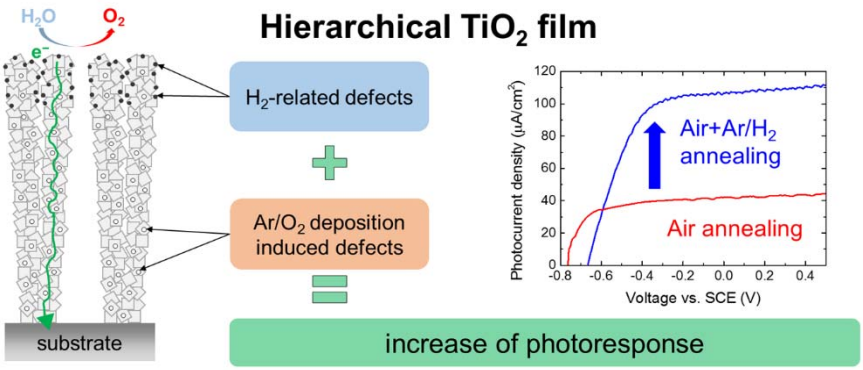

References

[1] J. Turner, G. Sverdrup, M.K. Mann, P.-C. Maness, B. Kroposki, M. Ghirardi, R.J. Evans, D. Blake, Renewable hydrogen production, Int. J. Energ. Res. 32 (2008) 379–407. doi:10.1002/er.1372.

[2] A. Kudo, Y. Miseki, Heterogeneous photocatalyst materials for water splitting, Chem. Soc. Rev. 38 (2008) 253–278. doi:10.1039/B800489G.

[3] A. Fujishima, K. Honda, Electrochemical Photolysis of Water at a Semiconductor Electrode, Nature. 238 (1972) 37–38. doi:10.1038/238037a0.

[4] H.M. Chen, C.K. Chen, R.-S. Liu, L. Zhang, J. Zhang, D.P. Wilkinson, Nano-architecture and material designs for water splitting photoelectrodes, Chem. Soc. Rev. 41 (2012) 5654–5671. doi:10.1039/C2CS35019J.

[5] P. Roy, S. Berger, P. Schmuki, TiO2 Nanotubes: Synthesis and Applications, Angew. Chem. Int. Ed. 50 (2011) 2904–2939. doi:10.1002/anie.201001374.

[6] Q. Zhang, G. Cao, Hierarchically structured photoelectrodes for dye-sensitized solar cells, J. Mater. Chem. 21 (2011) 6769–6774. doi:10.1039/C0JM04345A.

[7] B.I. Kharisov, O.V. Kharissova, B.O. García, Y.P. Méndez, I.G. de la Fuente, State of the art of nanoforest structures and their applications, RSC Adv. 5 (2015) 105507–105523. doi:10.1039/C5RA22738K.

[8] P. Gondoni, P. Mazzolini, V. Russo, A. Petrozza, A.K. Srivastava, A. Li Bassi, C.S. Casari, Enhancing light harvesting by hierarchical functionally graded transparent conducting Al-doped ZnO nano- and mesoarchitectures, Sol. Energy Mater. Sol. Cells. 128 (2014) 248–253. doi:10.1016/j.solmat.2014.05.035.

[9] R. Eason, ed., Pulsed Laser Deposition of Thin Films: Applications-Led Growth of Functional Materials, John Wiley & Sons, 2007. http://books.google.it/books?id=0jIO3cwkiOIC&dq.

[10] C.S. Casari, A. Li Bassi, Pulsed Laser Deposition of Nanostructured Oxides: from Clusters to Functional Films, in: W.T. Arkin (Ed.), Advances in Laser and Optics Research. Volume 7, Nova Science Publishers, 2011: pp. 65–100. https://www.novapublishers.com/catalog/product_info.php?products_id=38576&osCsid=6481ecde960c4230d2c81d7ef1ca3fad.

[11] F. Di Fonzo, C.S. Casari, V. Russo, M.F. Brunella, A. Li Bassi, C.E. Bottani, Hierarchically organized nanostructured TiO2 for photocatalysis applications, Nanotechnology. 20 (2009) 015604. doi:10.1088/0957-4484/20/1/015604.

[12] F. Sauvage, F. Di Fonzo, A. Li Bassi, C.S. Casari, V. Russo, G. Divitini, C. Ducati, C.E. Bottani, P. Comte, M. Grätzel, Hierarchical TiO2 Photoanode for Dye-Sensitized Solar Cells, Nano Lett. 10 (2010) 2562–2567. doi:10.1021/nl101198b.

[13] L. Passoni, F. Ghods, P. Docampo, A. Abrusci, J. Martí-Rujas, M. Ghidelli, G. Divitini, C. Ducati, M. Binda, S. Guarnera, A. Li Bassi, C.S. Casari, H.J. Snaith, A. Petrozza, F. Di Fonzo, Hyperbranched Quasi-1D Nanostructures for Solid-State Dye-Sensitized Solar Cells, ACS Nano. 7 (2013) 10023–10031. doi:10.1021/nn403979h.

[14] R. Matarrese, I. Nova, A.L. Li Bassi, C.S. Casari, V. Russo, Hierarchical nanostructured TiO2 films prepared by reactive pulsed laser position for photoelectrochemical water splitting, Chem. Eng. Trans. 41 (2014) 313–318. doi:10.3303/CET1441053.

[15] X. Chen, L. Liu, P.Y. Yu, S.S. Mao, Increasing Solar Absorption for Photocatalysis with Black Hydrogenated Titanium Dioxide Nanocrystals, Science. 331 (2011) 746–750. doi:10.1126/science.1200448.

[16] X. Chen, L. Liu, F. Huang, Black titanium dioxide (TiO2) nanomaterials, Chem. Soc. Rev. 44 (2015) 1861–1885. doi:10.1039/C4CS00330F.

[17] L. Liu, P.Y. Yu, X. Chen, S.S. Mao, D.Z. Shen, Hydrogenation and Disorder in Engineered Black TiO2, Phys. Rev. Lett. 111 (2013) 065505. doi:10.1103/PhysRevLett.111.065505.

[18] G. Wang, H. Wang, Y. Ling, Y. Tang, X. Yang, R.C. Fitzmorris, C. Wang, J.Z. Zhang, Y. Li, Hydrogen-Treated TiO2 Nanowire Arrays for Photoelectrochemical Water Splitting, Nano Lett. 11 (2011) 3026–3033. doi:10.1021/nl201766h.
[19] B. Chen, J.A. Beach, D. Maurya, R.B. Moore, S. Priya, Fabrication of black hierarchical TiO2 nanostructures with enhanced photocatalytic activity, RSC Adv. 4 (2014) 29443–29449. doi:10.1039/C4RA04260C.
[20] N. Liu, C. Schneider, D. Freitag, M. Hartmann, U. Venkatesan, J. Müller, E. Spiecker, P. Schmuki, Black TiO2 Nanotubes: Cocatalyst-Free Open-Circuit Hydrogen Generation, Nano Lett. 14 (2014) 3309–3313. doi:10.1021/nl500710j.
[21] P. Scherrer, Bestimmung der Größe und der inneren Struktur von Kolloidteilchen mittels Röntgenstrahlen, Göttinger Nachrichten Math. Phys. 2 (1918) 98–100.
[22] V. Ramakrishnan, H. Kim, J. Park, B. Yang, Cobalt oxide nanoparticles on TiO2 nanorod/FTO as a photoanode with enhanced visible light sensitization, RSC Adv. 6 (2016) 9789–9795. doi:10.1039/c5ra23200g.
[23] J. Han, Z. Liu, K. Guo, X. Zhang, T. Hong, B. Wang, AgSbS2 modified ZnO nanotube arrays for photoelectrochemical water splitting, Appl. Catal. B-Environ. 179 (2015) 61–68. doi:10.1016/j.apcatb.2015.05.008.
[24] B. Lucas-Granados, R. Sánchez-Tovar, R.M. Fernández-Domene, J. García-Antón, Study of the annealing conditions and photoelectrochemical characterization of a new iron oxide bi-layered nanostructure for water splitting, Sol. Energy Mater. Sol. Cells. 153 (2016) 68–77. doi:10.1016/j.solmat.2016.04.005.
[25] R.M. Fernández-Domene, R. Sánchez-Tovar, E. Segura-Sanchís, J. García-Antón, Novel tree-like WO3 nanoplatelets with very high surface area synthesized by anodization under controlled hydrodynamic conditions, Chem. Eng. J. 286 (2016) 59–67. doi:10.1016/j.cej.2015.10.069.
[26] Y. Cong, M. Chen, T. Xu, Y. Zhang, Q. Wang, Tantalum and aluminum co-doped iron oxide as a robust photocatalyst for water oxidation, Appl. Catal. B-Environ. 147 (2014) 733–740. doi:10.1016/j.apcatb.2013.10.009.
[27] M.-C. Huang, W.-S. Chang, J.-C. Lin, Y.-H. Chang, C.-C. Wu, Magnetron sputtering process of carbon-doped α-Fe2O3 thin films for photoelectrochemical water splitting, J. Alloy. Compd. 636 (2015) 176–182. doi:10.1016/j.jallcom.2015.02.166.
[28] R. Sánchez-Tovar, R.M. Fernández-Domene, D.M. García-García, J. García-Antón, Enhancement of photoelectrochemical activity for water splitting by controlling hydrodynamic conditions on titanium anodization, J. Power Sources. 286 (2015) 224–231. doi:10.1016/j.jpowsour.2015.03.174.
[29] D.B. Chrisey, G.K. Hubler, eds., Pulsed Laser Deposition of Thin Films, Wiley, 1994. https://books.google.it/books?id=0Oh_QgAACAAJ&dq.
[30] A. Bailini, F. Di Fonzo, M. Fusi, C.S. Casari, A. Li Bassi, V. Russo, A. Baserga, C.E. Bottani, Pulsed laser deposition of tungsten and tungsten oxide thin films with tailored structure at the nano- and mesoscale, Appl. Surf. Sci. 253 (2007) 8130–8135. doi:10.1016/j.apsusc.2007.02.145.
[31] O. Frank, M. Zukalova, B. Laskova, J. Kürti, J. Koltai, L. Kavan, Raman spectra of titanium dioxide (anatase, rutile) with identified oxygen isotopes (16, 17, 18), Phys. Chem. Chem. Phys. 14 (2012) 14567–14572. doi:10.1039/C2CP42763J.
[32] A. Li Bassi, D. Cattaneo, V. Russo, C.E. Bottani, E. Barborini, T. Mazza, P. Piseri, P. Milani, F.O. Ernst, K. Wegner, S.E. Pratsinis, Raman spectroscopy characterization of titania nanoparticles produced by flame pyrolysis: The influence of size and stoichiometry, J. Appl. Phys. 98 (2005) 074305. doi:10.1063/1.2061894.
[33] W.F. Zhang, Y.L. He, M.S. Zhang, Z. Yin, Q. Chen, Raman scattering study on anatase TiO2 nanocrystals, J. Phys. D: Appl. Phys. 33 (2000) 912. doi:10.1088/0022-3727/33/8/305.

[34] P. Mazzolini, V. Russo, C.S. Casari, T. Hitosugi, S. Nakao, T. Hasegawa, A. Li Bassi, Vibrational–Electrical Properties Relationship in Donor-Doped TiO2 by Raman Spectroscopy, J. Phys. Chem. C. 120 (2016) 18878–18886. doi:10.1021/acs.jpcc.6b05282.
[35] J.C. Parker, R.W. Siegel, Calibration of the Raman spectrum to the oxygen stoichiometry of nanophase TiO2, Appl. Phys. Lett. 57 (1990) 943–945. doi:10.1063/1.104274.
[36] A. Naldoni, M. Allieta, S. Santangelo, M. Marelli, F. Fabbri, S. Cappelli, C.L. Bianchi, R. Psaro, V. Dal Santo, Effect of Nature and Location of Defects on Bandgap Narrowing in Black TiO2 Nanoparticles, J. Am. Chem. Soc. 134 (2012) 7600–7603. doi:10.1021/ja3012676.
[37] F. De Angelis, C. Di Valentin, S. Fantacci, A. Vittadini, A. Selloni, Theoretical Studies on Anatase and Less Common TiO2 Phases: Bulk, Surfaces, and Nanomaterials, Chem. Rev. 114 (2014) 9708–9753. doi:10.1021/cr500055q.
[38] X. Liu, G. Zhu, X. Wang, X. Yuan, T. Lin, F. Huang, Progress in Black Titania: A New Material for Advanced Photocatalysis, Adv. Energy Mater. 6 (2016) 1600452. doi:10.1002/aenm.201600452.
[39] B. Zhou, M. Schulz, H.Y. Lin, S.I. Shah, J. Qu, C.P. Huang, Photoeletrochemical generation of hydrogen over carbon-doped TiO2 photoanode, Appl. Catal. B-Environ. 92 (2009) 41–49. doi:10.1016/j.apcatb.2009.07.026.
[40] A.J. Cowan, J. Tang, W. Leng, J.R. Durrant, D.R. Klug, Water Splitting by Nanocrystalline TiO2 in a Complete Photoelectrochemical Cell Exhibits Efficiencies Limited by Charge Recombination, J. Phys. Chem. C. 114 (2010) 4208–4214. doi:10.1021/jp909993w.
[41] F. Spadavecchia, S. Ardizzone, G. Cappelletti, L. Falciola, M. Ceotto, D. Lotti, Investigation and optimization of photocurrent transient measurements on nano-TiO2, J. Appll. Electrochem. 43 (2013) 217–225. doi:10.1007/s10800-012-0485-2.
[42] X.-M. Song, J.-M. Wu, M.-Z. Tang, B. Qi, M. Yan, Enhanced Photoelectrochemical Response of a Composite Titania Thin Film with Single-Crystalline Rutile Nanorods Embedded in Anatase Aggregates, J. Phys. Chem. C. 112 (2008) 19484–19492. doi:10.1021/jp8076886.
[43] Z. Xu, J. Yu, Visible-light-induced photoelectrochemical behaviors of Fe-modified TiO2 nanotube arrays, Nanoscale. 3 (2011) 3138–3144. doi:10.1039/C1NR10282F.
[44] K. Zhang, X.-J. Shi, J.K. Kim, J.H. Park, Photoelectrochemical cells with tungsten trioxide/Mo-doped BiVO4 bilayers, Phys. Chem. Chem. Phys. 14 (2012) 11119–11124. doi:10.1039/C2CP40991G.
[45] S.U.M. Khan, M. Al-Shahry, W.B. Ingler, Efficient Photochemical Water Splitting by a Chemically Modified n-TiO2, Science. 297 (2002) 2243–2245. doi:10.1126/science.1075035.
[46] O.K. Varghese, C.A. Grimes, Appropriate strategies for determining the photoconversion efficiency of water photoelectrolysis cells: A review with examples using titania nanotube array photoanodes, Sol. Energy Mater. Sol. Cells. 92 (2008) 374–384. doi:10.1016/j.solmat.2007.11.006.
[47] N. Liu, C. Schneider, D. Freitag, E.M. Zolnhofer, K. Meyer, P. Schmuki, Noble-Metal-Free Photocatalytic H2 Generation: Active and Inactive “Black” TiO2 Nanotubes and Synergistic Effects, Chem. Eur. J. 22 (2016) 13810–13814. doi:10.1002/chem.201602714.
[48] G. Divitini, O. Stenzel, A. Ghadirzadeh, S. Guarnera, V. Russo, C.S. Casari, A. Li Bassi, A. Petrozza, F. Di Fonzo, V. Schmidt, C. Ducati, Nanoscale Analysis of a Hierarchical Hybrid Solar Cell in 3D, Adv. Funct. Mater. 24 (2014) 3043–3050. doi:10.1002/adfm.201302836.
[49] H. Cui, W. Zhao, C. Yang, H. Yin, T. Lin, Y. Shan, Y. Xie, H. Gu, F. Huang, Black TiO2 nanotube arrays for high-efficiency photoelectrochemical water-splitting, J. Mater. Chem. A. 2 (2014) 8612–8616. doi:10.1039/C4TA00176A.
[50] S. Hoang, S.P. Berglund, N.T. Hahn, A.J. Bard, C.B. Mullins, Enhancing Visible Light Photo-oxidation of Water with TiO2 Nanowire Arrays via Cotreatment with H2 and NH3: Synergistic Effects between Ti3+ and N, J. Am. Chem. Soc. 134 (2012) 3659–3662. doi:10.1021/ja211369s.

[51] J.-Y. Shin, J.H. Joo, D. Samuelis, J. Maier, Oxygen-Deficient TiO2−δ Nanoparticles via Hydrogen Reduction for High Rate Capability Lithium Batteries, Chem. Mater. 24 (2012) 543–551. doi:10.1021/cm2031009.
[52] Z. Lu, C.-T. Yip, L. Wang, H. Huang, L. Zhou, Hydrogenated TiO2 Nanotube Arrays as High-Rate Anodes for Lithium-Ion Microbatteries, ChemPlusChem. 77 (2012) 991–1000. doi:10.1002/cplu.201200104.
[53] S. Zhang, S. Zhang, B. Peng, H. Wang, H. Yu, H. Wang, F. Peng, High performance hydrogenated TiO2 nanorod arrays as a photoelectrochemical sensor for organic compounds under visible light, Electrochem. Commun. 40 (2014) 24–27. doi:10.1016/j.elecom.2013.12.013.